Wang *et al. Energy Mater.* **2025**, *5*, 500012
DOI: 10.20517/energymater.2024.51

Energy Materials

Article

Open Access

Multifunctional zinc silicate coating layer for high-performance aqueous zinc-ion batteries

Keliang Wang[1,*], **Nina Baule**[1], **Hong Jin**[2,*], **Hui Qiao**[3,*], **Aaron Hardy**[1], **Thomas Schuelke**[1], **Qi Hua Fan**[4,*]

[1]Fraunhofer USA, Inc. Center for Midwest, East Lansing, MI 48824, USA.
[2]Suzhou Research Institute, Xi'an Jiaotong University, Suzhou 215123, Jiangsu, China.
[3]Key Laboratory of Eco-textiles, Ministry of Education, Jiangnan University, Wuxi 214122, Jiangsu, China.
[4]Department of Electrical Engineering and Computer Engineering & Department of Chemical Engineering and Materials Science, Michigan State University, East Lansing, MI 48824, USA.

Correspondence to: Dr. Keliang Wang, Fraunhofer USA, Inc. Center for Midwest, East Lansing, Michigan 48824, USA. E-mail: kwang@fraunhofer.org; Dr. Hong Jin, Suzhou Research Institute, Xi'an Jiaotong University, Suzhou 215123, Jiangsu, China. E-mail: jhjinhong@mail.xjtu.edu.cn; Prof. Hui Qiao, Key Laboratory of Eco-textiles, Ministry of Education, Jiangnan University, Wuxi 214122, Jiangsu, China. E-mail: huiqiao@jiangnan.edu.cn; Prof. Qi Hua Fan, Department of Electrical Engineering and Computer Engineering & Department of Chemical Engineering and Materials Science, Michigan State University, East Lansing, MI 48824, USA. E-mail: qfan@msu.edu

How to cite this article: Wang, K.; Baule, N.; Jin, H.; Qiao, H.; Hardy, A.; Schuelke, T.; Fan, Q. H. Multifunctional zinc silicate coating layer for high-performance aqueous zinc-ion batteries. *Energy Mater.* **2025**, *5*, 500012. https://dx.doi.org/10.20517/energymater.2024.51

Received: 24 May 2024 **First Decision:** 18 Jun 2024 **Revised:** 28 Jun 2024 **Accepted:** 16 Jul 2024 **Published:** 8 Jan 2025

Academic Editor: Jiazhao Wang **Copy Editor:** Ping Zhang **Production Editor:** Ping Zhang

Abstract

Dendrite growth during the continuous charge/discharge process is a serious problem that leads to internal short circuits in aqueous zinc-ion batteries. Herein, a multifunctional zinc silicate polymer lithium polysilicate (LSO) was proposed to address the issues. LSO can prevent direct contact between electrolytes and zinc anodes, thereby suppressing severe dendrite growth. Its mechanically stable structure can restrain the stress release to further stabilize the electrode. In addition, LSO is chemically bonded to zinc anodes to ensure superior overall stability compared to other surface coatings. Moreover, LSO anodes exhibit outstanding electrolyte wettability and corrosion resistance, with strong adhesion properties. *In-situ* optical microscopy observation demonstrates its stability during charge/discharge process. Symmetrical cells using the Zn-LSO anode exhibited long cycling life of 833, 455, 344, and 260 h with low overpotentials of 66, 80, 118, and 141 mV at current densities of 0.5, 1, 3 and 5 mA cm^{-2}, respectively. Full cells coupled with a MnO_2 cathode showed a high-capacity reversibility of up to 234 mAh g^{-1} and outstanding rate performance at different current densities. This study demonstrates that LSO coating is a promising method for enhancing the electrochemical performance of zinc-ion batteries.

Keywords: Dendrite-free, zinc-ion battery, zinc silicate polymer, multifunctional, high-performance

INTRODUCTION

Rechargeable lithium-ion and lithium-metal batteries have achieved remarkable energy/power density and charge/discharge performance in recent years[1,2]. While improving the operation safety of these batteries is under active research, the cost and source of the electrode materials remain a concern. Aqueous rechargeable batteries, including Zn^{2+}, Mg^{2+}, Ca^{2+}, and Al^{3+}, are promising alternatives. These batteries use materials that are abundant and environmentally friendly and have achieved considerable power density at a low cost[3-6]. Furthermore, the neutral electrolyte (pH = 7) has excellent ionic conductivity and the battery fabrication can be performed in an atmosphere environment, which is particularly advantageous over sensitive organic-electrolyte-based batteries. Among aqueous rechargeable batteries, zinc-ion batteries with a zinc metal anode possess unique characteristics and are particularly attractive because of their high theoretical capacity of 820 mAh g^{-1}, relatively low electrochemical potential [-0.762 V *vs.* standard hydrogen electrode (SHE)], and highly operational safety[7-9].

Recently, various metallic Zn-based anode battery systems, such as Zn/Manganese oxide, Zn/Vanadium oxide, and Zn/hexacyanoferrates[10-13], have demonstrated excellent electrochemical performance. However, the reported aqueous zinc-ion batteries suffer from a limited life span and considerable capacity fading due to dendrite growth on the Zn anode during Zn plating/stripping as the batteries charge/discharge[14-17]. Zinc dendrites not only cause internal short circuits by piercing the separator, but also reduce the utilization of Zn[15,18,19]. Therefore, achieving a dendrite-free Zn anode is crucial for maintaining stable reversibility in rechargeable Zn batteries.

The growth of zinc dendrites includes two steps: nucleation and subsequent crystal growth driven by an electric field. These two steps are determined by the nucleation overpotential and plateau overpotential during the Zn plating process. Lower overpotential reduces the resistance during nucleation and growth processes, improving zinc plating quality with less energy consumption[20,21]. These overpotentials are closely linked to the ion distribution and electric field at the reaction interface. Therefore, considerable efforts have been devoted to tuning the electron or ion behavior to achieve a dendrite-free Zn anode from the perspectives of intrinsic Zn anodes, electrolytes, and current collectors. Reported work can be categorized into three groups: (i) deposit a protective layer [e.g., AgF/polyvinyl alcohol (PVA), nanoporous $CaCO_3$, nano-ZrO_2, or polyamide layers][21-26] on a bare Zn to suppress the Zn evolution; (ii) add an additive to the electrolyte {e.g., LiCl, Na_2SO_4, Zinc (II) bis(trifluoromethylsulfonyl)imide [$Zn(TFSI)_2$] and $Zn[CF_3SO_3]_2$}[27-31] to enable even zinc deposition by adjusting the adsorption of zinc ions on the anode surface or enabling the formation of an *in-situ* transition protection layer on the Zn anode surface. This layer provides a shielding effect to suppress the dendrite growth[32]; (iii) create a nanostructured current collector (e.g., 3D porous copper skeleton, 3D flexible carbon nanotubes, or Ti_3C_2Tx MXene paper) as the zinc host to promote uniform zinc deposition on the anode surface and effectively equalize the surface electric field[18,33-35]. Among these strategies, modifying the Zn anode with a protective layer is straightforward and more effective. However, most of current surface coating optimization methods focus on designing mechanically protective film to block the dendrite growth. Herein, we propose a multifunctional zinc anode protection strategy that considers mechanical strength, electrode surface compatibility, and overall stability.

This coating layer is constructed by a facile and low-cost approach. The buffer layer is formed on the surface of zinc *via* a strong cross-link reaction with lithium polysilicate (LSO) that features strong adhesion and high corrosion resistance. As illustrated in Figure 1, zinc dendrites can be effectively suppressed by this robust coating, leading to a long cycling life with low overpotential for the symmetric cells. Combining the LSO/Zn anode with a MnO_2 cathode, we achieved superior battery capacity at different currents from low to high. Cycling stability is significantly improved for the Zn/LSO-MnO_2 battery. The entire process is simple

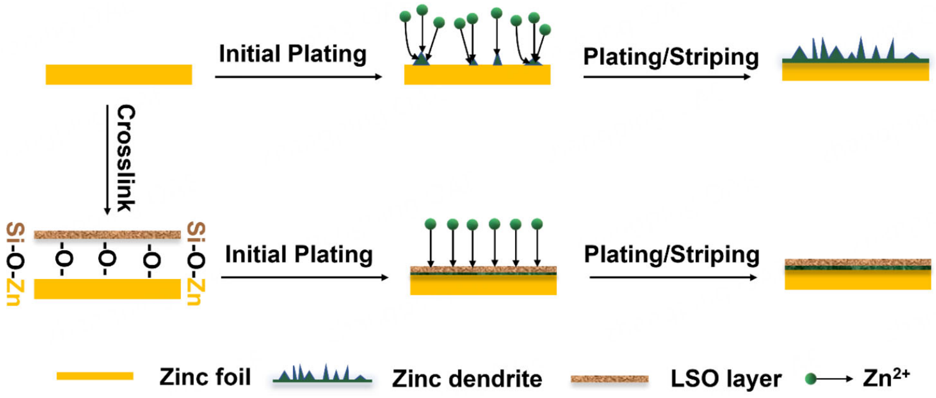

Figure 1. Schematic illustration of the comparison before and after LSO modification. LSO: Lithium polysilicate.

and efficient, offering an economic approach to fabricating dendrite-free zinc anodes.

EXPERIMENTAL

Preparation of Zn-LSO anode

The initial substrates were made of pure Zinc foil of 10 μm thickness and cut into round disks 12.7 mm in diameter. Then, the bare Zinc disks were coated with 150 μL LSO solution ($Li_2Si_5O_{11}$, Sigma-Aldrich, Inc.) at varying concentrations (0.5 *wt*%, 1 *wt*% and 1.5 *wt*%). The coated disks were dried overnight to allow full cross-link. The coated substrates were denoted as Zn-LSO-x, where x represented the concentration of LSO.

Preparation of α-MnO_2 cathode

First, 0.0304 g Manganese sulfate monohydrate ($MnSO_4 \cdot H_2O$, Fisher Scientific Inc.) was dispersed into 60 mL deionized (DI) water, and then 10 mL 0.5 M sulfuric acid (H_2SO_4, Fisher Scientific Inc.) was added under vigorous stirring. After 20 min, 20 mL potassium permanganate (0.1 M, $KMnO_4$) was added to the solution, followed by 1-h ultrasonication. The mixture was then transferred into a 100 mL polytetrafluoroethylene (PTFE) lined autoclave and reacted at 120 °C for 12 h. Afterward, the sediment was separated using a centrifuge and washed with DI water till the pH reached 7. The resulting product was collected, dried overnight at 60 in an oven, and denoted as α-MnO_2.

Materials characterizations

The morphologies and structures of the anode and cathode materials were characterized using a scanning electron microscope (SEM) (6610LV, JEOL, Japan) equipped with energy dispersive spectroscopy (EDS). An *in-situ* optical cell was used to construct symmetric cells with pure Zn and Zn-LSO-1 anodes for monitoring the Zn plating process using an optical microscope (Nikon microscope). X-ray photoelectron spectroscopy (XPS) analysis was conducted on an SSX-100 system (Surface Science Laboratories, Inc.) equipped with a monochromated Al Kα X-ray source. The crystal structure of the samples was examined by X-ray diffraction (XRD) (Rigaku Smartlab, Rigaku Americas, Inc. United States).

Assembly of symmetric cells and MnO_2-based full cells

The symmetric cells consisted of two electrodes of Zinc or Zn-LSO-x, a piece of glass fiber separator, and 150 μL 2 M zinc sulfate ($ZnSO_4$) electrolyte, assembled into CR2025 coin-type-cells. These cells were cycled at various current densities of 0.5, 1, 3 and 5 mA cm^{-2} at a fixed specific capacity of 0.1 mAh cm^{-2}.

The MnO_2-based full cells were assembled using Zinc or Zn-LSO-x as an anode and MnO_2 as a cathode. The cathode was prepared by mixing MnO_2, acetylene black and Polyvinylidene fluoride (PVDF) with a mass ratio of 7:2:1, using N-Methyl-2-pyrrolidone (NMP, Fisher Scientific Inc.) as a solvent. The resulting slurry was applied onto stainless-steel foil using a film applicator, and then dried at 120 °C in a vacuum oven for 24 h to remove excess solvent. The mass loading and thickness of the coated electrode materials were 1 mg cm^{-2} and 10 μm, respectively.

The Zn/MnO_2 and Zn-LSO-x/MnO_2 cells (bare Zinc or Zn-LSO-x anode and MnO_2 cathode) were assembled in the same procedure of the symmetric cells, but using 2 M ZnSO4 + 0.2 M $MnSO_4$ as electrolyte. All batteries were set for four hours before the electrochemical measurements.

Electrochemical characterization

The electrochemical measurements, including cyclic voltammetry (CV), linear polarization and electrochemical impedance spectroscopy (EIS), were conducted on a potentiostat (PGSTAT128N, Metrohm) for both symmetric and full cells. Galvanostatic charge/discharge measurements were conducted using a Neware battery tester (BTS series, NEWARE, China).

RESULTS AND DISCUSSION

Surface modification of zinc anode is critical for improving the cycle stability and capacity retention of zinc-ion batteries. In pursuit of a high-performance zinc-ion battery, we engineered a zinc silicate coating layer with mechanical and chemical stability on the surface of zinc anodes. The zinc silicate polymer protection layer was formed *via* the following steps: (i) The initial curing reaction involves concentrating the silicate/zinc film by evaporating the solvent, water (reaction Supplementary S1); (ii) Insolubilization occurs as the silicate matrix forms with zinc ions from the surface of zinc foil (reaction Supplementary S2); (iii) Further hydrolysis of silicate in the presence of carbonic acid formed from atmospheric CO_2 dissolved in water (reaction Supplementary S3); (iv) Production of polysilicic acid (reaction Supplementary S4), which then reacts with zinc ions to form a zinc silicate polymer with a 3D structure (inorganic matrix, reaction Supplementary S5). The resulting zinc silicate polymer exhibits excellent mechanical strength due to the strong combination of -Zn-O-Si-O-Zn- bonds. SEM was used to examine the surface morphologies of bare zinc and LSO-coated Zn (LSO-0.5, LSO-1 and LSO-1.5). The bare zinc had a smooth surface with texture [Figure 2A], while a rough surface with random pores was observed in Zn-LSO-1 [Figure 2B], and incomplete coating was observed for both Zn-LSO-0.5 and Zn-LSO-1.5 [Supplementary Figure 1]. In the cross-sectional SEM images [Figure 2C and D], a coating layer with a thickness of ~2 μm could be clearly observed for Zn-LSO-1, in contrast to the 10 μm thick bare zinc and irregular coatings for Zn-LSO-0.5 and Zn-LSO-1.5 [Supplementary Figure 1C and F]. In addition, the coating layer of Zn-LSO-1 was recognized in the element mapping, revealing a uniform distribution of Zn, O and Si [Supplementary Figure 2]. The wettability of the electrolyte (2 M $ZnSO_4$) on the surface of bare zinc foil and Zn-LSO-1 was assessed using contact angle measurements. As depicted in Figure 2E and F, the Zn-LSO-1 electrode showed much better wettability to electrolyte with a significantly reduced contact angle of 51.1° compared to 107.7° for bare zinc, suggesting the significantly enhanced hydrophilicity/wettability of electrolyte on the electrode surface. The enhanced hydrophilicity not only favors the electrolyte penetration and ion transports to the interfaces but also enables reduced interfacial free energy between the electrode and electrolyte, and consequently leads to homogeneous Zn plating and nucleation with low charge transfer resistance during the Zn stripping/plating process[36,37]. Among the Zn-LSO-0.5, Zn-LSO-1 and Zn-LSO-1.5, the coating layer of Zn-LSO-1 was believed to be most effective in suppressing dendrites due to its mechanical strength and the micropores that offer smooth channels for zinc ion transportation.

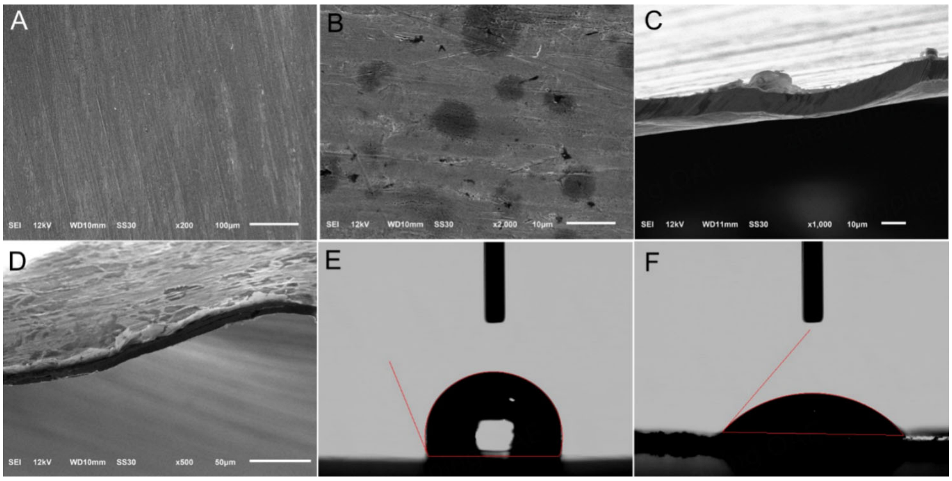

Figure 2. SEM images of (A) bare zinc; (B) Zn-LSO-1; and cross-sectional images of (C) bare zinc and (D) Zn-LSO-1; Contact angle for the (E) bare Zn and (F) Zn-LSO-1 with 2 M $ZnSO_4$ electrolyte. SEM: Scanning electron microscope; LSO: Lithium polysilicate.

To examine the stability of the modified zinc in electrolyte, both bare zinc and Zn-LSO foil were soaked in 2 M $ZnSO_4$ electrolyte. As illustrated in Figure 3A, the bare zinc surface was severely corroded and became thinner and fragile with an obvious color change to dark gray, indicating side reactions happened and damaged the zinc foil. In contrast, the Zn-LSO surface showed no significant difference and the entire piece retained its integrity even after bending, indicating a limited corrosion occurred. Furthermore, linear polarization was conducted to investigate the corrosion resistance of the zinc foil before and after LSO modification. Corrosion resistance can be indexed by two criteria: corrosion potential ($E_{corr.}$) and corrosion current density ($j_{corr.}$). Small j_{corr} and/or large positive $E_{corr.}$ values are indications of superior corrosion resistance. As depicted in Figure 3B and Supplementary Figure 3, the LSO-modified zinc foils generally showed a lower j_{corr} and more positive $E_{corr.}$ than that of the bare zinc. The specific values are summarized in Table 1, showing that the Zn-LSO-1 had the lowest $j_{corr.}$ (1.53×10^{-6} A cm^{-2}) and most positive $E_{corr.}$ (-0.973 V *vs.* Ag/AgCl) in comparison with 1.53×10^{-6} A cm^{-2} and -0.991 V for bare zinc, indicating that the LSO coating could effectively improve the overpotential of HER and subsequently improve the corrosion resistance in $ZnSO_4$ electrolyte because of its electrochemical inertness. Interestingly, Zn-LSO-1 exhibited the smallest charge transfer resistance among all prepared electrodes [Figure 3C and Supplementary Figure 4], demonstrating fast charge transfer with stable Zn plating/stripping kinetics.

To investigate the suppression of dendrite growth during zinc plating/stripping process, a cell with a quartz window for *in-situ* optical microscopic monitoring was assembled and integrated into an electrochemical working station. A high current density of 5 mA cm^{-2} with an areal capacity of 0.1 mAh cm^{-2} was applied to Zn/Zn and Zn-LSO-1/Zn-LSO-1 symmetrical cells under charge/discharge cycling up to 60 min, with optical images being recorded at 20 min intervals [Figure 4A and B]. It is worth noting that the bare zinc electrode surface is always uneven at microscale, and the sharp points become preferential nucleation sites of zinc dendrite. The zinc surface remained in its initial state for about 20 minutes. Then, corrosion near the edge and plenty of nuclei on the Zn surface were observed. The corrosion became severe and large dendrites evolved from the nuclei after ~ 60 min. In contrast, no obvious corrosion or dendrite growth was observed on the surface of Zn-LSO-1 during the entire process (Note: the dark round spots are the signs of corrosion for the uncoated zinc/bare zinc on the top flat area of the cell). Meanwhile, a lower and more stable voltage hysteresis was observed for Zn-LSO-1 during the real-time recording in comparison with the fluctuated profiles for the bare zinc electrode [Figure 4C]. The results confirmed the superior anti-corrosion and dendrite-suppression performance of Zn-LSO-1.

Table 1. A summary of corrosion current density ($j_{corr.}$) and potential ($E_{corr.}$) of Zn, Zn-LSO-0.5, Zn-LSO-1 and Zn-LSO-1.5 anodes

Entry	$j_{corr.}$ (A cm^{-2})	$E_{corr.}$ (V *vs.* Ag/AgCl)
Zn	6.1×10^{-4}	-0.991
Zn-LSO-0.5	4.08×10^{-4}	-0.991
Zn-LSO-1	1.53×10^{-6}	-0.973
Zn-LSO-1.5	4.23×10^{-4}	-0.997

LSO: Lithium polysilicate; $E_{corr.}$: Corrosion potential; $j_{corr.}$: Corrosion current density.

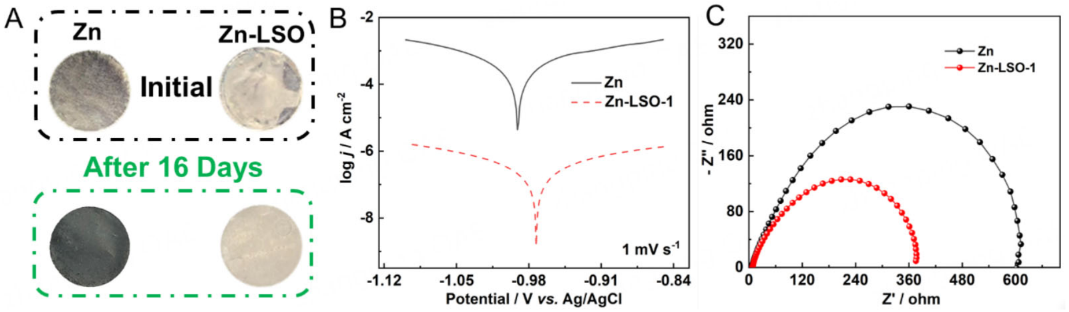

Figure 3. (A) Digital images of bare zinc and Zn-LSO-1 before and after being soaked in 2 M $ZnSO_4$ for 16 days; (B) Tafel curves of Zn and Zn-LSO-1 anode; (C) Nyquist plots of Zn and Zn-LSO-1 anode. LSO: Lithium polysilicate.

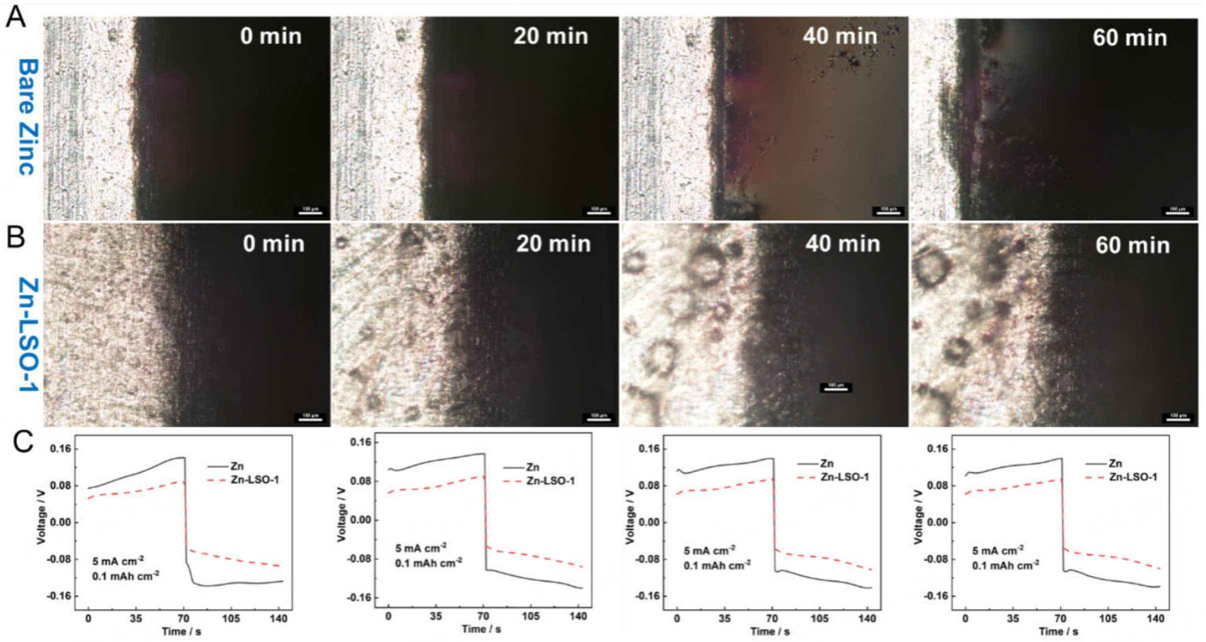

Figure 4. *In-situ* optical microscope photos of the interface between electrolyte and electrode for symmetrical cells (A) Zn and (B) Zn-LSO-1, during zinc plating/stripping process at a current density of 5 mA cm^{-2} with an areal capacity of 0.1 mAh cm^{-2}; (C) The real time voltage profiles of symmetrical Zn and Zn-LSO-1 cells. LSO: Lithium polysilicate.

The XPS was conducted to further understand the interface combination between Zn substrate and LSO for Zn-LSO-1. Elements of Zn, Si, and O were all detected in the survey spectra which was consistent with the composition of the formed zinc silicate polymer [Figure 5A]. Figure 5B showed that the high-resolution spectra of Si 2p were deconvoluted into two main peaks. The one located at 102.7 eV was associated with

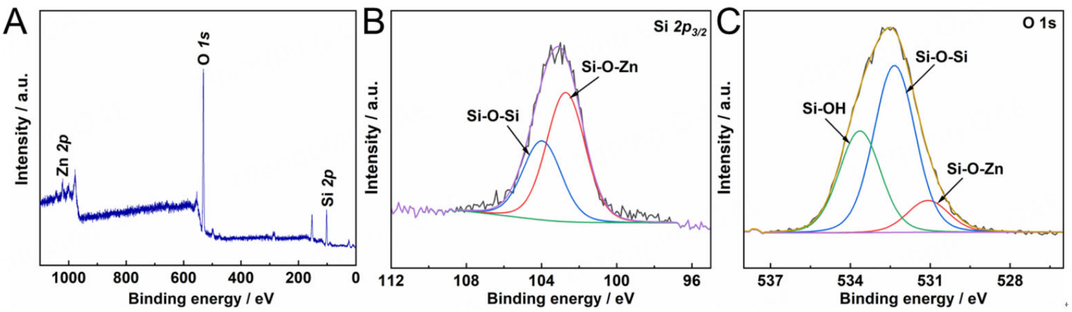

Figure 5. (A) XPS spectra of Zn-LSO-1; The high-resolution XPS spectra of (B) Zn 2p; (C) Si 2p and O 1s regions of Zn-LSO-1. LSO: Lithium polysilicate; XPS: X-ray photoelectron spectroscopy.

the Si-O-Zn bond, while the other one located at 103.9 eV was attributed to Si-O-Si[38]. Furthermore, the O 1s spectra were deconvoluted into three peaks with binding energies of 531.3, 532.4 and 533.6 eV [Figure 5C], corresponding to Si-OH, Si-O-Si, and Si-O-Zn species, respectively[38,39], aligning with the analysis of Si 2p spectra. Summarizing the aforementioned XPS analysis, it is strongly confirmed the bonding status between LSO and Zn substrate is due to the formation of zinc silicate polymer coating layers.

Symmetrical cells using bare zinc, Zn-LSO-0.5, Zn-LSO-1 and Zn-LSO-1.5 anodes were prepared to test the stability of Zn stripping/plating behaviors. The cells were charged/discharged at different current densities with a fixed areal capacity of 0.1 mAh cm^{-2}. In comparison with the bare zinc electrode, the Zn-LSO-x electrode exhibited much smaller voltage hysteresis and longer cycling life. Specifically, the Zn-LSO-1/Zn-LSO-1 batteries were cycled for 835, 455 and 260 h at current densities of 0.5, 1 and 5 mA cm^{-2}, respectively [Figure 6A, B and C] which is significantly longer than that of Zn/Zn batteries (150, 148, and 50 h at current densities of 0.5, 1 and 5 mA cm^{-2}, respectively). In addition, smaller voltage hysteresis values of 66, 80 and 141 mV were observed for Zn-LSO-1/Zn-LSO-1 batteries compared with 159, 168, and 228 mV for bare Zn/Zn batteries at current densities of 0.5, 1 and 3 mA cm^{-2}, respectively [Figure 6D, E and F]. At a high current density of 3 mA cm^{-2} [Figure 6G and H, Supplementary Figure 5A-D], the symmetrical cells with Zn-LSO-1 electrodes exhibited the lowest overpotential of 118 mV and a stable cycling life of up to 344 h, compared to 261 mV and 110 h for the bare zinc electrode. The superior cycling stability of the symmetrical cells with Zn-LSO-1 was also demonstrated at different current densities of 0.5, 1 and 5 mA cm^{-2}. The cycling of Zn/Zn batteries under all current densities exhibited a sudden increase in voltage oscillation, indicating the separator was pierced by zinc dendrites. In contrast, stable voltage hysteresis with negligible change in the voltage oscillation amplitude was observed for Zn-LSO-1/Zn-LSO-1 batteries before failure, indicating reversible Zn plating/stripping behaviors for Zn-LSO-1 electrode. It is worth noting that both the voltage hysteresis and cycling life of Zn-LSO-1 electrodes were superior to the previously reported anodes for zinc-ion batteries [Supplementary Table 1]. Therefore, Zn-LSO-1 was promising for achieving a low overpotential and ultralong lifetime due to its effective suppression of zinc dendrites.

As a demonstration for the real application of the Zn-LSO-1 anode, a full cell with an α-MnO$_2$ cathode was assembled using a CR3025 cell. The SEM images of the MnO$_2$ are shown in Figure 7A and Supplementary Figure 6A, revealing an urchin-like nanostructure with abundant nanowires. XRD was conducted to identify the crystal structure of the MnO$_2$. As shown in Supplementary Figure 6B, the characteristic peaks located at 12.7°, 18.1°, 28.8°, 37.5°, 42.1°, 49.9°, 56.2°, and 60.3° corresponded to (110), (200), (310), (211), (301), (411), (600), and (521) planes, respectively. The peaks match well with the standard diffraction patterns of α-MnO$_2$ (JCPDS# 44-0141).

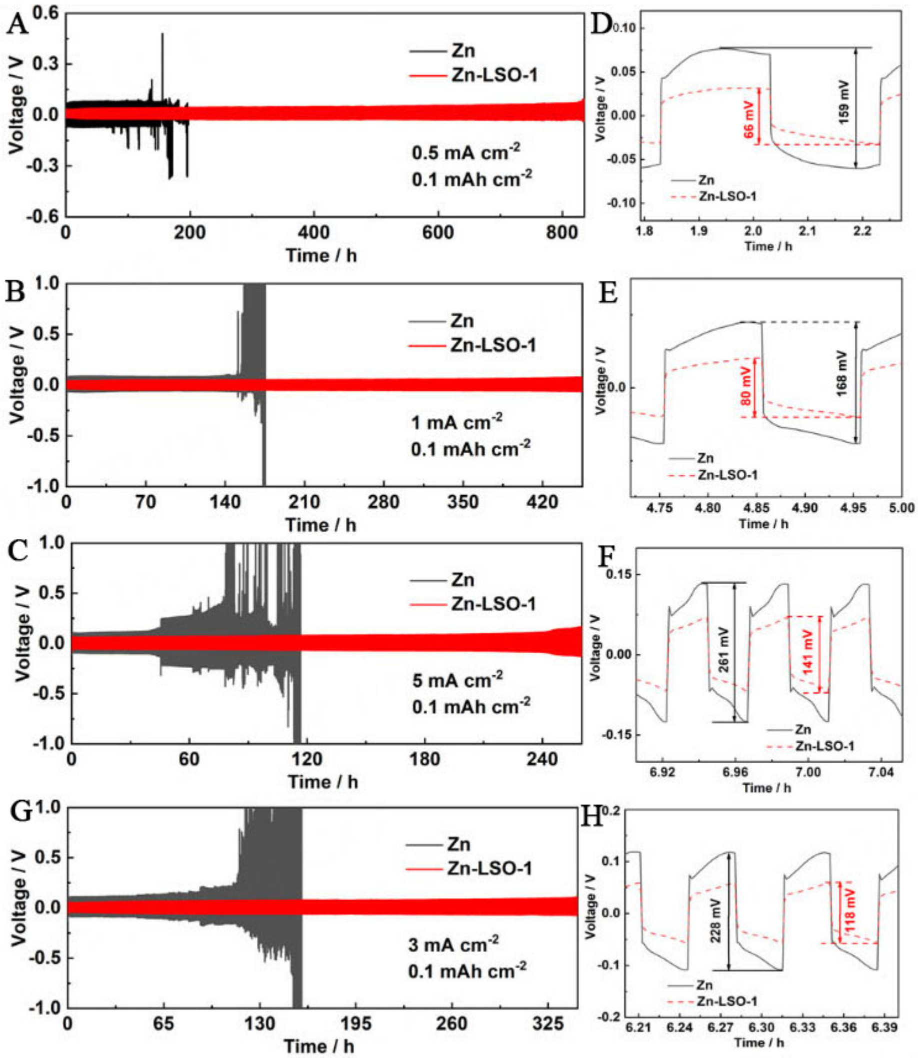

Figure 6. Galvanostatic cycling stability and corresponding voltage profiles of symmetrical Zn and Zn-LSO-1 cells at various current densities: (A, D) 0.5, (B, E) 1, (G, H) 3 and (C, F) 5 mA cm^{-2}, with an areal capacity of 0.1 mAh cm^{-2}. LSO: Lithium polysilicate.

For the electrochemical measurements, CV tests were performed at a scanning rate of 2 mV s^{-1} with a voltage range of 0.8 - 1.9 V for both Zn/MnO_2 and Zn-LSO-1/MnO_2 cells. Two characteristic peaks were observed around ~ 1.3 and 1.2 V in the cathodic sweep, which originated from the two-step reduction from Mn^{4+} to Mn^{3+} and then to Mn^{2+}[25]. An anodic peak appeared at ~ 1.65 V during the anodic sweep, which can be attributed to the reverse oxidation reaction[25]. Compared to the Zn/MnO_2 battery, the Zn-LSO-1/MnO_2 battery possessed a slightly enhanced current density and the anodic/cathodic peaks shifted to more negative/positive voltages, respectively. A smaller voltage difference between the pair of cathodic/anodic peaks for the MnO_2 and Zn-LSO-1 electrodes was more conducive to Zn storage/delivery than the Zn electrode[40-42]. These redox peaks were consistent with the plateaus observed in the galvanostatic charge/discharge profiles of both Zn/MnO_2 and Zn-LSO-1/MnO_2 batteries [Figure 7B]. Overall, the charge/discharge voltage profiles were similar. However, the Zn-LSO-1/MnO_2 battery had a lower charge plateau and higher discharge plateau than the Zn/MnO_2 battery. These results indicated a reduced voltage gap and polarization of the Zn-LSO-1/MnO_2 battery due to the improved kinetics of Zn deposition and dissolution on the anode. At a constant charge/discharge current density of 0.2 A g^{-1}, the Zn-LSO-1/MnO_2 battery

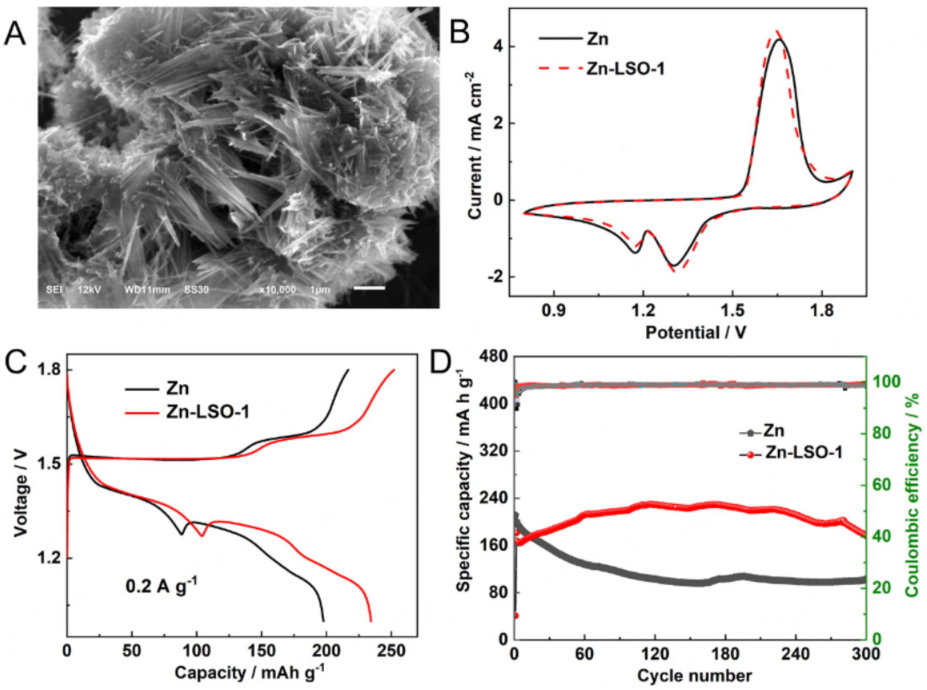

Figure 7. (A) SEM image of MnO_2; (B) CV curves of Zn/MnO_2 and Zn-LSO-1/MnO_2 cells at a scanning rate of 0.2 mV s^{-1}; (C) galvanostatic charge and discharge potential profiles and (D) cycling stability performance of Zn/MnO_2 and Zn-LSO-1/MnO_2 cells at a current density of 1 A g^{-1}. LSO: Lithium polysilicate; SEM: Scanning electron microscope; CV: Cyclic voltammetry.

delivered a discharge capacity of 234 mAh g^{-1}, significantly higher than the Zn-LSO-1/MnO_2 battery (198 mAh g^{-1}). Galvanostatic charge/discharge cycles at different current densities (0.2, 0.5, 1, and 1 A g^{-1}) further confirmed that the Zn-LSO-1/MnO_2 batteries consistently outperformed the Zn/MnO_2 battery in discharge capacity [Supplementary Figure 7A and B]. In Figure 7C, the galvanostatic discharge-charge (GDC) profile at the current density of 0.2 A g^{-1} for the first cycle was presented, revealing discharge/charge capacities of 234.5 and 197 for Zn/MnO_2 and Zn-LSO-1/MnO_2 batteries, respectively.

The long-term cycling performance of both Zn/MnO_2 and Zn-LSO-1/MnO_2 batteries was investigated at a current density of 1 A g^{-1} [Figure 7D]. The Zn-LSO-1/MnO_2 battery consistently exhibited higher capacity than the Zn/MnO_2 battery. The capacity of the Zn-LSO-1/MnO_2 battery gradually increased from 181 mA g^{-1} to 230 mA g^{-1} after approximately 60 cycles, and maintained a capacity of 176 mA g^{-1} after 300 cycles, with a capacity retention of 97% and coulombic efficiency (CE) of ~ 98.7%. In contrast, the capacity of the Zn/MnO_2 battery significantly decreased from 200 mA g^{-1} to 100 mA g^{-1}, resulting in a loss of ~ 50% after 300 cycles. In addition, a capacity variation was observed in the initial cycles for Zn-LSO-1, attributed to the initial activation process driven by the bulk-nanocrystalline evolution[43-45]. Rate performance of Zn and Zn-LSO-1-based full cells at various current densities ranging from 0.1 to 2 A g^{-1} was also studied [Supplementary Figure 8]. Overall, the Zn/MnO_2 battery exhibited lower rate capacities and worse retention compared to the Zn-LSO-1/MnO_2 battery. Especially the Zn-LSO-1/MnO_2 battery delivered high capacities of 240, 221, 175, and 104 mAh g^{-1}, corresponding to the current densities of 0.2, 0.5, 1, and 2 A g^{-1}, respectively. These results highlighted the excellent electrochemical performance of the Zn-LSO-1 anode, indicating its promising potential for practical applications.

CONCLUSION

A zinc silicate polymer coating formed *via* effective cross-link reactions between LSO and zinc foil can directly serve as an anode for aqueous zinc-ion batteries. With the optimum LSO concentration, the zinc silicate polymer coating effectively suppressed dendrite growth and exhibited excellent anti-corrosion performance, as evidenced by improved wettability to electrolyte, low $j_{corr.}$ and positive going E_{corr}. Symmetric cells with the Zn-LSO anode demonstrate excellent cycling performance, characterized by long lifetime and low overpotential at a wide range of current densities compared with bare zinc anodes. Moreover, full cells using Zn-LSO anodes coupled with MnO_2 cathodes present outstanding capacity performance and cycling stability. The Zn-LSO anode is economic and promising for practical Zn battery applications. This study opens a promising approach to constructing dendrite-free anodes for other aqueous metal-ion batteries.

DECLARATIONS

Authors' contributions

Conception, and characterizations, and manuscript drafting: Wang, K.
Materials characterization: Baule, N.; Hardy A.
Review and editing: Jin, H.; Qiao, H.; Schuelkea, T.; Fan, Q. H.

Availability of data and materials

The data is available from the corresponding authors upon reasonable request.

Financial support and sponsorship

This work was financially supported by the National Science Foundation (#1724941 and #1917577) and Fraunhofer USA, and National Natural Science Foundation of China (No. 22109085).

Conflicts of interest

All authors declared that there are no conflicts of interest.

Ethical approval and consent to participate

Not applicable.

Consent for publication

Not applicable.

Copyright

REFERENCES

1. Huang, Z.; Ren, J.; Zhang, W.; et al. Protecting the Li-metal Anode in a Li-O_2 battery by using boric acid as an SEI-forming additive. *Adv. Mater.* **2018**, *30*, e1803270. DOI
2. Chen, L.; Fan, X.; Ji, X.; Chen, J.; Hou, S.; Wang, C. High-energy Li metal battery with lithiated host. *Joule* **2019**, *3*, 732-44. DOI
3. Adil, M.; Sarkar, A.; Roy, A.; Panda, M. R.; Nagendra, A.; Mitra, S. Practical aqueous calcium-ion battery full-cells for future stationary storage. *ACS. Appl. Mater. Inter.* **2020**, *12*, 11489-503. DOI
4. Janoschka, T.; Martin, N.; Hager, M. D.; Schubert, U. S. An aqueous redox-flow battery with high capacity and power: the TEMPTMA/MV system. *Angew. Chem. Int. Ed. Engl.* **2016**, *55*, 14427-30. DOI PubMed
5. Pasta, M.; Wessells, C. D.; Huggins, R. A.; Cui, Y. A high-rate and long cycle life aqueous electrolyte battery for grid-scale energy storage. *Nat. Commun.* **2012**, *3*, 1149. DOI
6. Gheytani, S.; Liang, Y.; Wu, F.; et al. An aqueous Ca-ion battery. *Adv. Sci.* **2017**, *4*, 1700465. DOI
7. Zeng, X.; Hao, J.; Wang, Z.; Mao, J.; Guo, Z. Recent progress and perspectives on aqueous Zn-based rechargeable batteries with mild aqueous electrolytes. *Energy. Storage. Mater.* **2019**, *20*, 410-37. DOI
8. Verma, V.; Kumar, S.; Manalastas, W.; Satish, R.; Srinivasan, M. Progress in rechargeable aqueous zinc-and aluminum-ion battery

electrodes: challenges and outlook. *Adv. Sustain. Syst.* **2019**, *3*, 1800111. DOI

9. Jia, H.; Wang, Z.; Tawiah, B.; et al. Recent advances in zinc anodes for high-performance aqueous Zn-ion batteries. *Nano. Energy.* **2020**, *70*, 104523. DOI
10. He, P.; Yan, M.; Zhang, G.; et al. Layered VS_2 nanosheet-based aqueous Zn ion battery cathode. *Adv. Energy. Mater.* **2017**, *7*, 1601920. DOI
11. He, B.; Man, P.; Zhang, Q.; et al. Conversion synthesis of self-standing potassium zinc hexacyanoferrate arrays as cathodes for high-voltage flexible aqueous rechargeable sodium-ion batteries. *Small* **2019**, *15*, e1905115. DOI
12. Zhang, N.; Dong, Y.; Jia, M.; et al. Rechargeable aqueous Zn-V_2O_5 battery with high energy density and long cycle life. *ACS. Energy. Lett.* **2018**, *3*, 1366-72. DOI
13. Chen, S.; Lan, R.; Humphreys, J.; Tao, S. Salt-concentrated acetate electrolytes for a high voltage aqueous Zn/MnO_2 battery. *Energy. Storage. Mater.* **2020**, *28*, 205-15. DOI
14. Cao, Z.; Zhuang, P.; Zhang, X.; Ye, M.; Shen, J.; Ajayan, P. M. Strategies for dendrite-free anode in aqueous rechargeable zinc ion batteries. *Adv. Energy. Mater.* **2020**, *10*, 2001599. DOI
15. Zhang, Q.; Luan, J.; Tang, Y.; Ji, X.; Wang, H. Interfacial design of dendrite-free zinc anodes for aqueous zinc-ion batteries. *Angew. Chem. Int. Ed.* **2020**, *59*, 13180-91. DOI
16. Hong, Z.; Ahmad, Z.; Viswanathan, V. Design principles for dendrite suppression with porous polymer/aqueous solution hybrid electrolyte for Zn metal anodes. *ACS. Energy. Lett.* **2020**, *5*, 2466-74. DOI
17. Lee, J.; Kim, R.; Kim, S.; et al. Dendrite-free Zn electrodeposition triggered by interatomic orbital hybridization of Zn and single vacancy carbon defects for aqueous Zn-based flow batteries. *Energy. Environ. Sci.* **2020**, *13*, 2839-48. DOI
18. Zeng, Y.; Zhang, X.; Qin, R.; et al. Dendrite-free zinc deposition induced by multifunctional CNT frameworks for stable flexible Zn-ion batteries. *Adv. Mater.* **2019**, *31*, e1903675. DOI
19. An, G.; Hong, J.; Pak, S.; et al. 2D metal Zn nanostructure electrodes for high-performance Zn ion supercapacitorss. *Adv. Energy. Mater.* **2020**, *10*, 1902981. DOI
20. Liu, X.; Lu, Q.; Yang, A.; Qian, Y. High ionic conductive protection layer on Zn metal anode for enhanced aqueous zinc-ion batteries. *Chinese. Chem. Lett.* **2023**, *34*, 107703. DOI
21. Li, J.; Yin, X.; Duan, F.; et al. Pure amorphous and ultrathin phosphate layer with superior ionic conduction for zinc anode protection. *ACS. Nano.* **2023**, *17*, 20062-72. DOI
22. Liang, P.; Yi, J.; Liu, X.; et al. Highly reversible Zn anode enabled by controllable formation of nucleation sites for Zn-based batteries. *Adv. Funct. Mater.* **2020**, *30*, 1908528. DOI
23. Zhao, K.; Wang, C.; Yu, Y.; et al. Ultrathin surface coating enables stabilized zinc metal anode. *Adv. Mater. Inter.* **2018**, *5*, 1800848. DOI
24. Deng, C.; Xie, X.; Han, J.; et al. A sieve-functional and uniform-porous kaolin layer toward stable zinc metal anode. *Adv. Funct. Mater.* **2020**, *30*, 2000599. DOI
25. Kang, L.; Cui, M.; Jiang, F.; et al. Nanoporous $CaCO_3$ coatings enabled uniform Zn stripping/plating for long-life zinc rechargeable aqueous batteries. *Adv. Energy. Mater.* **2018**, *8*, 1801090. DOI
26. Zhao, Z.; Zhao, J.; Hu, Z.; et al. Long-life and deeply rechargeable aqueous Zn anodes enabled by a multifunctional brightener-inspired interphase. *Energy. Environ. Sci.* **2019**, *12*, 1938-49. DOI
27. Xu, W.; Zhao, K.; Huo, W.; et al. Diethyl ether as self-healing electrolyte additive enabled long-life rechargeable aqueous zinc ion batteries. *Nano. Energy.* **2019**, *62*, 275-81. DOI
28. Wang, F.; Borodin, O.; Gao, T.; et al. Highly reversible zinc metal anode for aqueous batteries. *Nat. Mater.* **2018**, *17*, 543-9. DOI
29. Zhang, Q.; Luan, J.; Fu, L.; et al. The three-dimensional dendrite-free zinc anode on a copper mesh with a zinc-oriented polyacrylamide electrolyte additive. *Angew. Chem. Int. Ed. Engl.* **2019**, *58*, 15841-7. DOI
30. Li, W.; Wang, K.; Zhou, M.; Zhan, H.; Cheng, S.; Jiang, K. Advanced low-cost, high-voltage, long-life aqueous hybrid sodium/zinc batteries enabled by a dendrite-free zinc anode and concentrated electrolyte. *ACS. Appl. Mater. Inter.* **2018**, *10*, 22059-66. DOI
31. Han, J.; Lee, J.; Lee, H.; et al. In-situ coating of metal fluoride/polymer bi-layer protection for dendrite-free, anti-corrosive Zn-metal anode. *Chem. Eng. J.* **2024**, *485*, 149881. DOI
32. Guo, X.; Zhang, Z.; Li, J.; et al. Alleviation of dendrite formation on zinc anodes via electrolyte additives. *ACS. Energy. Lett.* **2021**, *6*, 395-403. DOI
33. Yin, Y.; Wang, S.; Zhang, Q.; et al. Endrite-free zinc deposition induced by tin-modified multifunctional 3D host for stable zinc-based flow battery. *Adv. Mater.* **2020**, *32*, e1906803. DOI
34. Tian, Y.; An, Y.; Wei, C.; et al. Flexible and free-standing $Ti_3C_2T_x$ MXene@Zn paper for dendrite-free aqueous zinc metal batteries and nonaqueous lithium metal batteries. *ACS. Nano.* **2019**, *13*, 11676-85. DOI
35. Ci, J.; Cao, C.; Kuga, S.; Shen, J.; Wu, M.; Huang, Y. Improved performance of microbial fuel cell using esterified corncob cellulose nanofibers to fabricate air-cathode gas diffusion layer. *ACS. Sustainable. Chem. Eng.* **2017**, *5*, 9614-8. DOI
36. Hao, J.; Li, X.; Zhang, S.; et al. Designing dendrite-free zinc anodes for advanced aqueous zinc batteries. *Adv. Funct. Mater.* **2020**, *30*, 2001263. DOI
37. Guo, W.; Cong, Z.; Guo, Z.; et al. Dendrite-free Zn anode with dual channel 3D porous frameworks for rechargeable Zn batteries. *Energy. Storage. Mater.* **2020**, *30*, 104-12. DOI
38. Dong, G.; Tian, G.; Gong, L.; et al. Mesoporous zinc silicate composites derived from iron ore tailings for highly efficient dye

removal: structure and morphology evolution. *Micropor. Mesopor. Mater.* **2020**, *305*, 110352. DOI
39. Zhang, Y.; Zhu, L.; Chen, L.; Liu, L.; Ye, G. Influence of magnesia on demoulding strength of colloidal silica-bonded castables. *Rev. Adv. Mater. Sci.* **2019**, *58*, 32-7. DOI
40. Huang, J.; Tang, X.; Liu, K.; Fang, G.; He, Z.; Li, Z. Interfacial chemical binding and improved kinetics assisting stable aqueous Zn-MnO_2 batteries. *Mater. Today. Energy.* **2020**, *17*, 100475. DOI
41. Wang, S. B.; Ran, Q.; Yao, R. Q.; et al. Lamella-nanostructured eutectic zinc-aluminum alloys as reversible and dendrite-free anodes for aqueous rechargeable batteries. *Nat. Commun.* **2020**, *11*, 1634. DOI
42. Ming, J.; Guo, J.; Xia, C.; Wang, W.; Alshareef, H. N. Zinc-ion batteries: materials, mechanisms, and applications. *Mater. Sci. Eng. R. Rep.* **2019**, *135*, 58-84. DOI
43. Liu, M.; Zhao, Q.; Liu, H.; et al. Tuning phase evolution of β-MnO_2 during microwave hydrothermal synthesis for high-performance aqueous Zn ion battery. *Nano. Energy.* **2019**, *64*, 103942. DOI
44. Zhao, Q.; Chen, X.; Wang, Z.; et al. Unravelling H^+/Zn^{2+} synergistic intercalation in a novel phase of manganese oxide for high-performance aqueous rechargeable battery. *Small* **2019**, *15*, e1904545. DOI
45. Liao, Y.; Chen, H.; Yang, C.; et al. Unveiling performance evolution mechanisms of MnO_2 polymorphs for durable aqueous zinc-ion batteries. *Energy. Storage. Mater.* **2022**, *44*, 508-16. DOI